



OPEN ACCESS

Original research

# Targeting m<sup>6</sup>A reader YTHDF1 augments antitumour immunity and boosts anti-PD-1 efficacy in colorectal cancer

Yi Bao,<sup>1</sup> Jianning Zhai,<sup>1</sup> Huarong Chen ,<sup>2</sup> Chi Chun Wong,<sup>1</sup> Cong Liang,<sup>3</sup> Yanqiang Ding,<sup>1</sup> Dan Huang,<sup>1</sup> Hongyan Gou,<sup>1</sup> Danyu Chen,<sup>1</sup> Yasi Pan,<sup>1</sup> Wei Kang ,<sup>4</sup> Ka Fai To,<sup>4</sup> Jun Yu <sup>1</sup>

► Additional supplemental material is published online only. To view, please visit the journal online (<http://dx.doi.org/10.1136/gutjnl-2022-328845>).

<sup>1</sup>Department of Medicine and Therapeutics, The Chinese University of Hong Kong, Hong Kong, Hong Kong

<sup>2</sup>Anaesthesia and Intensive Care, Chinese University of Hong Kong, Hong Kong, Hong Kong, Hong Kong

<sup>3</sup>Institute of Precision Medicine, the First Affiliated Hospital, Sun Yat-sen University, Guang Zhou, China

<sup>4</sup>Department of Anatomical and Cellular Pathology, The Chinese University of Hong Kong, Hong Kong, Hong Kong

## Correspondence to

Dr Jun Yu, Medicine and Therapeutics, The Chinese University of Hong Kong, Hong Kong, Hong Kong; [junyu@cuhk.edu.hk](mailto:junyu@cuhk.edu.hk)

YB and JZ contributed equally.

Received 5 October 2022  
Accepted 17 January 2023  
Published Online First  
30 January 2023



© Author(s) (or their employer(s)) 2023. Re-use permitted under CC BY-NC. No commercial re-use. See rights and permissions. Published by BMJ.

**To cite:** Bao Y, Zhai J, Chen H, *et al.* *Gut* 2023;**72**:1497–1509.

## ABSTRACT

**Objective** The role of N<sup>6</sup>-methyladenosine (m<sup>6</sup>A) in tumour immune microenvironment (TIME) remains understudied. Here, we elucidate function and mechanism of YTH N<sup>6</sup>-methyladenosine RNA binding protein 1 (YTHDF1) in colorectal cancer (CRC) TIME.

**Design** Clinical significance of YTHDF1 was assessed in tissue microarrays (N=408) and TCGA (N=526) cohorts. *YTHDF1* function was determined in syngeneic tumours, intestine-specific *Ythdf1* knockin mice, and humanised mice. Single-cell RNA-seq (scRNA-seq) was employed to profile TIME. Methylated RNA immunoprecipitation sequencing (MeRIP-seq), RNA sequencing (RNA-seq) and ribosome sequencing (Ribo-seq) were used to identify YTHDF1 direct targets. Vesicle-like nanoparticles (VNPs)-encapsulated *YTHDF1*-siRNA was used for *YTHDF1* silencing in vivo.

**Results** *YTHDF1* expression negatively correlated with interferon- $\gamma$  gene signature in TCGA-CRC. Concordantly, YTHDF1 protein negatively correlated with CD8<sup>+</sup> T-cell infiltration in independent tissue microarrays cohorts, implying its role in TIME. Genetic depletion of *Ythdf1* augmented antitumour immunity in CT26 (MSS-CRC) and MC38 (MSI-H-CRC) syngeneic tumours, while *Ythdf1* knockin promoted an immunosuppressive TIME facilitating CRC in azoxymethane-dextran sulphate-sodium or *Apc*<sup>Min/+</sup> models. scRNA-seq identified reduction of myeloid-derived suppressor cells (MDSCs), concomitant with increased cytotoxic T cells in *Ythdf1* knockout tumours. Integrated MeRIP-seq, RNA-seq and Ribo-seq revealed p65/Rela as a YTHDF1 target. YTHDF1 promoted p65 translation to upregulate CXCL1, which increased MDSC migration via CXCL1-CXCR2 axis. Increased MDSCs in turn antagonised functional CD8<sup>+</sup> T cells in TIME. Importantly, targeting YTHDF1 by CRISPR (Clustered Regularly Interspaced Short Palindromic Repeats) or VNPs-si*YTHDF1* boosted anti-PD1 efficacy in MSI-H CRC, and overcame anti-PD1 resistance in MSS CRC.

**Conclusion** YTHDF1 impairs antitumour immunity via an m<sup>6</sup>A-p65-CXCL1/CXCR2 axis to promote CRC and serves as a therapeutic target in immune checkpoint blockade therapy.

## WHAT IS ALREADY KNOWN ON THIS TOPIC

- ⇒ N<sup>6</sup>-methyladenosine (m<sup>6</sup>A) modification plays crucial roles in cancer by regulating RNA splicing, translation and degradation.
- ⇒ YTH N<sup>6</sup>-methyladenosine RNA binding protein 1 (YTHDF1) is a m<sup>6</sup>A reader that determines the fate of m<sup>6</sup>A modified mRNA. However, its potential role in colorectal cancer (CRC) immune microenvironment (TIME) is understudied.

## WHAT THIS STUDY ADDS

- ⇒ High YTHDF1 expression is inversely correlated with interferon- $\gamma$  gene signatures and CD8<sup>+</sup> T cell infiltration in multiple cohorts of patient with CRC.
- ⇒ Single-cell sequencing revealed that YTHDF1 contributes to an immunosuppressive TIME with increased infiltration of MDSCs and reduced effector T cells.
- ⇒ YTHDF1 promotes tumour growth via an immunosuppressive TIME in syngeneic mice, intestine-specific *Ythdf1* knockin mice, and CD34<sup>+</sup> humanised mice of CRC.
- ⇒ Integrative methylated RNA immunoprecipitation sequencing, RNA-seq and Ribo-seq revealed p65/RELA as a YTHDF1 target, leading to increased expression of the cytokine CXCL1, a chemoattractant for MDSCs via CXCL1-CXCR2 axis.
- ⇒ YTHDF1-recruited MDSCs antagonise effector CD8<sup>+</sup> and CD4<sup>+</sup> T cells in TIME of CRC, thereby promoting tumourigenesis.
- ⇒ Targeting of YTHDF1 by gene knockout or nanoparticle-encapsulated *YTHDF1*-siRNA synergised with anti-PD1 to suppress the growth of microsatellite instability-high (MSI-H) CRC, and overcomes anti-PD1 resistance in microsatellite stable (MSS) CRC.

## HOW THIS STUDY MIGHT AFFECT RESEARCH, PRACTICE OR POLICY

- ⇒ Therapeutic targeting of YTHDF1 is a potential strategy to sensitise both MSI-H and MSS CRC to immune checkpoint blockade therapy.
- ⇒ YTHDF1 serves as a prognostic factor in patients with CRC.

## INTRODUCTION

Colorectal cancer (CRC) is one of the most common cancers worldwide. It is still a deadly cancer with a 5-year survival rate lower than 20% among metastatic patients.<sup>1</sup> Immune checkpoint blockade (ICB) has shown beneficial effects to patients with CRC. However, only a minor fraction of patients with microsatellite instability-high (MSI-H) or deficient mismatch repair are responsive to ICB.<sup>1,2</sup> Therefore, understanding the molecular mechanisms of immune evasion in CRC and identifying therapeutic strategies that could improve the response to immunotherapies for patients with proficient mismatch repair, microsatellite instability-low, or microsatellite stable (MSS) CRC are crucial.

N<sup>6</sup>-methyladenosine (m<sup>6</sup>A) is one of the most abundant RNA modifications, with an estimated 3–5 m<sup>6</sup>A sites on each mRNA molecule.<sup>3</sup> m<sup>6</sup>A modification is regulated by writers, erasers and readers. m<sup>6</sup>A writers catalyse m<sup>6</sup>A formation, consisting of a protein complex of METTL3, METTL14 and WTAP. m<sup>6</sup>A markers are also actively removed by erasers including FTO and ALKBH5. m<sup>6</sup>A readers, such as YTH N<sup>6</sup>-methyladenosine RNA binding protein 1/2/3 (YTHDF1/2/3), YTHDC1/2 and IGF2BP1/2/3 bind to m<sup>6</sup>A-modified mRNAs to determine the fate of m<sup>6</sup>A-modified mRNA.<sup>3</sup> m<sup>6</sup>A regulators such as YTHDF1, METTL3 and ALKBH5 have been intensively studied in cancer. Upregulation of YTHDF1 has been reported to be associated with poor prognosis in various cancer types<sup>4–6</sup> and YTHDF1 could promote tumorigenesis and cancer metastasis.<sup>4–6</sup> However, the role of YTHDF1 in tumour immune microenvironment (TIME) is largely unclear.

Here, we identified that *YTHDF1* expression negatively correlated with the interferon gamma (IFN- $\gamma$ ) signature in The Cancer Genome Atlas (TCGA) CRC dataset. Furthermore, we demonstrated for the first time that genetic depletion of *Ythdf1* in murine CRC cells of both MSS and MSI-H could induce accumulation of MDSCs and inhibit the infiltration of T cells in syngeneic CRC mice and humanised mice. On the contrary, intestine-specific *Ythdf1* knockin drives an immunosuppressive TIME that facilitates spontaneous CRC formation. By integrative analyses of methylated RNA immunoprecipitation sequencing (MeRIP-seq), RNA-seq and Ribo-seq, a YTHDF1-m<sup>6</sup>A-p65-CXCL1 axis was identified as the mechanism of YTHDF1-induced immunosuppression, leading to the recruitment of MDSCs to suppress effector cells such as functional CD8<sup>+</sup> T cells. Moreover, targeting of YTHDF1 by CRISPR or vesicle-like nanoparticles (VNPs)-siRNA enhanced anti-PD1 efficacy in both MSS and MSI-H models, supporting YTHDF1 as a therapeutic target in the immunotherapy of CRC.

## METHODS

### Clinical samples

Cohort I comprised 206 patients with surgically excised CRC tissues, which derived from Prince of Wales Hospital, Hong Kong. Cohort II was Beijing cohort, consisting of 202 patients with CRC. Paraffinised sample of these two cohorts were used to establish the tissue microarrays (TMA). The clinicopathological features of the two cohorts were provided in online supplemental tables S1 and S2. Informed consent was obtained for all patients.

### Humanised mouse models

Four-to-five week-old NOD.Cg-Prkdcscid Il2rgtm1Wjl/SzJ (NSG) mice were exposed to total body gamma irradiation (150–170 cGy/animal) and then intravenously injected with  $5 \times 10^4$  human cord blood-derived CD34<sup>+</sup> haematopoietic stem cells (STEMCELL) within 24 hours. The percentage of human CD45 positive cells in CD34<sup>+</sup> humanised mice was monitored at weeks 8 and 16 by flow cytometry, after CD34<sup>+</sup> haematopoietic stem cells transplantation. CD34<sup>+</sup> humanised mice with >20% human CD45<sup>+</sup> cells in blood were used for establishment of xenografts. All animal studies followed the guidelines approved by the Animal Experimentation Ethics Committee of The Chinese University of Hong Kong.

### Murine CRC models with intestinal-specific *Ythdf1* knockin

Intestinal-specific *Ythdf1* knockin mice (*Ythdf1*<sup>loxpl/loxpl</sup>-*CDX2-cre*) were established. Six to eight weeks old transgenic mice were intraperitoneally injected with tamoxifen (100 mg/kg) to activate *Ythdf1* overexpression. For azoxymethane-dextran sulphate-sodium (AOM/DSS) CRC mice model, 7–8 week-old mice were injected intraperitoneally with AOM (10 mg/kg body weight) (#A5486, Sigma-Aldrich), and the mice were given water containing 1.5% dextran sulfate sodium (DSS) (#9011-18-1, MP Biomedicals) for 4 days, 5 days after AOM injection. The regular drinking water was used for the following 2 weeks. DSS treatment was given for an additional 2 cycles, and the mice were sacrificed on day 80. For *Apc*<sup>Min/+</sup> CRC mice model, *Ythdf1*<sup>loxpl/loxpl</sup>*CDX2-cre* mice were crossed with *Apc*<sup>Min/+</sup> mice to generate *Apc*<sup>Min/+</sup> *Ythdf1*<sup>loxpl/loxpl</sup>*CDX2-cre*, all mice were sacrificed after 16 weeks. All animal experiments in this study were approved by the Animal Experimentation Ethics Committee of CUHK and Xiamen University.

### TCGA data analysis

Colorectal adenocarcinoma TCGA data (TCGA, PanCancer Atlas) were acquired from cBioPortal (<https://www.cbioportal.org/>).<sup>7,8</sup> Coexpression data performed with Spearman's correlation in 526 samples was downloaded also from cBioPortal. Genes correlated with *YTHDF1* in mRNA expression were subjected to gene set enrichment analysis (GSEA\_4.1.0).<sup>9</sup> The normalised enrichment scores for IFN- $\gamma$  signature response was shown. For analysing the association between expression of *YTHDF1* and CXCL1 family members, data from stage IV patients were used. High expression tumour was defined with a z-score higher than 0.7, while low expression with a z-score lower than -0.7. The associations were determined with  $\chi^2$  tests.

### Statistical analysis

All measurements were acquired using independent samples rather than collected with repeated measurements. GraphPad Prism V.8 (GraphPad Software; San Diego, California) was used for data analysis, and the data were shown as means  $\pm$  SD, unless stated otherwise. Two-tailed student's t-test was used to conduct statistical analysis, unless stated otherwise. A p value < 0.05 was regarded as statistically significant.

Additional methods are provided in the online supplemental material.

## RESULTS

### *YTHDF1* is associated with reduced IFN- $\gamma$ -related gene signatures and poor prognosis in CRC

By analysing copy number variations of 21 known m<sup>6</sup>A regulators using TCGA data, we identified that *YTHDF1* is the top

m<sup>6</sup>A regulator displaying copy number gain or amplification in nearly 80% of CRC tumours (online supplemental figure S1A). Such an increase of copy number is also concordant with upregulation of mRNA expression (online supplemental figure S1A) and protein expression (online supplemental figure S1C), implicating that YTHDF1 functions in promoting CRC. To establish a link between antitumour immunity and m<sup>6</sup>A regulators, we then performed GSEA to analyse the correlation between m<sup>6</sup>A regulators with IFN- $\gamma$  response gene signature. We found that *YTHDF1* showed a striking negative correlation ( $q < 0.0001$ ) with the IFN- $\gamma$  response pathway (online supplemental figure S1B). Of note, IFN- $\gamma$  response is associated with the induction of antitumour immunity<sup>10,11</sup> and responsiveness to ICB therapy.<sup>12,13</sup> Consistently, *YTHDF1* expression strongly anticorrelated with an 18 IFN- $\gamma$ -related gene signature (figure 1A), which predicts anti-PD1 responsiveness in multiple cancer types.<sup>14,15</sup> Furthermore, expression of *CD8A* or *CD8<sup>+</sup>* T cell signature<sup>16</sup> is negatively correlated with *YTHDF1* expression (online supplemental figure S1D). In agreement with TCGA data, IHC staining of TMA from our CRC TMA cohorts showed that high protein expression of YTHDF1 was correlated with low infiltration of *CD8<sup>+</sup>* T cells in cohort I ( $p < 0.001$ ,  $r = -0.248$ ,  $n = 206$ ) (figure 1B) and cohort II ( $p < 0.0001$ ,  $r = -0.269$ ,  $n = 202$ ) (figure 1C). These data strongly imply that m<sup>6</sup>A reader YTHDF1 is associated with impaired antitumour immunity and reduced ICB treatment efficacy.

In agreement with the notion that low *CD8<sup>+</sup>* T cell infiltration is associated with poor prognosis,<sup>17</sup> high expression of YTHDF1 (54.3%, 100/184) predicted poor survival of patients with CRC ( $p < 0.01$ , log-rank test) (online supplemental figure S1E,F). Multivariate Cox regression analysis validated that YTHDF1 was an independent prognostic factor for CRC in cohort II (HR, 1.764; 95% CI 1.058 to 2.939;  $p < 0.05$ ) (online supplemental figure S1F). These findings were further verified in cohort I by multivariate Cox regression analysis (online supplemental figure S1E).

### Single-cell transcriptomics reveal YTHDF1-induced immunosuppression

To investigate the role of YTHDF1 in regulating antitumour immunity, we used the CRISPR-Cas9 system to knockout *Ythdf1* (*Ythdf1*-KO) in MC38 murine MSI-H CRC cells and injected the cells to syngeneic C57BL6 mice (figure 1D). We found that both tumour volume and weight were reduced by knockout of *Ythdf1* compared with control (NC) (figure 1E). To ask if *Ythdf1*-KO impact TIME, we isolated *CD45<sup>+</sup>* immune cells from the tumours and performed single cell RNA-seq (scRNA-seq) (NC: 1480 cells; *Ythdf1*-KO: 1816 cells). Tumours with *Ythdf1*-KO exhibited strong reduction of granulocytic myeloid-derived suppressor cells (G-MDSCs, cluster 3) and neutrophils compared with NC group (figure 1F and online supplemental figure S2A). In contrast, T cells and NK cells were largely increased in *Ythdf1*-KO tumours (figure 1F and online supplemental figure S2A). We further reclustered T and NK cells into *CD4<sup>+</sup>* T, *CD8<sup>+</sup>* T, NKT and NK cell subsets, and identified that they were simultaneously increased in *Ythdf1*-KO tumours compared with controls (figure 1F). We thus speculated that YTHDF1 can suppress the antitumour immunity through inducing MDSC accumulation. Functional markers of MDSCs, *Il1b*, *Arg2*, *Cxcr2* and *Ccr2* were examined, and these genes were mainly enriched in MDSC clusters (cluster 3 and cluster 4), especially from tumours without *Ythdf1* knockout (figure 1G). Thus, data from this syngeneic model supports an immunosuppressive function of YTHDF1 in CRC.

### *Ythdf1* knockout reduces MDSCs but increases cytotoxic T cell infiltration

To validate our findings in scRNA-seq analyses, the composition of tumour-infiltrating immune cells in MC38 syngeneic mice was determined by flow cytometry. We confirmed that *Ythdf1* knockout significantly suppressed tumour weight and volume (figure 1C), and flow cytometry revealed that *Ythdf1* knockout decreased MDSCs, but increased *CD8<sup>+</sup>* T and *CD4<sup>+</sup>* T cells in tumours (figure 1H,I). Of MDSCs, G-MDSCs were the predominant subset, and knockout of *Ythdf1* led to the remarkable reduction of G-MDSCs (figure 1I). In line with the immunosuppressive function of MDSCs, we observed significant increase of functional T cells, including IFN- $\gamma$ <sup>+</sup> *CD8<sup>+</sup>* T cells, Granzyme B<sup>+</sup> *CD8<sup>+</sup>* T cells, and IFN- $\gamma$ <sup>+</sup> *CD4<sup>+</sup>* T cells in *Ythdf1*-KO group (figure 1H,J).

We next performed the experiment in CT26 (MSS-CRC) with *Ythdf1*-KO to validate the role of YTHDF1 in regulating antitumour immunity. As expected, *Ythdf1*-KO led to reduced tumour volume and weight (figure 2A,B) in CT26 syngeneic mice, together with reduced functional T cells and accumulation of MDSCs (figure 2C,D). Immunofluorescence staining confirmed the decreased infiltration of MDSCs (*CD11b<sup>+</sup>*Gr-1<sup>+</sup>) in both MC38 and CT26 syngeneic tumours on *Ythdf1* knockout (figure 2E and online supplemental figure S2B). Collectively, *Ythdf1* depletion in CRC cells reduced MDSCs and increased functional T cell infiltration. These findings are in line with clinical data demonstrating YTHDF1 anticorrelated with *CD8<sup>+</sup>* T cell and IFN- $\gamma$ -related signatures (figure 1A–C, online supplemental figure S1B,D).

We asked if the attenuated tumour formation in *Ythdf1*-KO was dependent on *CD8<sup>+</sup>* T cell antitumour immunity. To address this, we depleted *CD8<sup>+</sup>* T cells with an anti-*CD8* antibody in the MC38 syngeneic model. Consistent with our hypothesis, depletion of *CD8<sup>+</sup>* T cells restored growth of *Ythdf1*-KO tumours (figure 2F,G), demonstrating that tumour-suppressing function of *Ythdf1*-KO was dependent, at least partially, on *CD8<sup>+</sup>* T cells. This was confirmed in CT26 syngeneic mice showing that anti-*CD8* antibody treatment rescued arrested tumour growth in *Ythdf1*-KO group (figure 2H,I). Depletion of *CD8<sup>+</sup>* T cells by anti-*CD8* antibody was confirmed by flow cytometry (online supplemental figure S3A,B). Together, *Ythdf1* knockout suppresses CRC growth through the induction of *CD8<sup>+</sup>* T cell-dependent antitumour immunity.

### Intestine-specific *Ythdf1* knockin promotes colorectal tumourigenesis and suppresses antitumour immunity in mice

To verify the role of YTHDF1 in spontaneous colorectal tumourigenesis, we generated intestine-specific *Ythdf1* knockin mice (*Ythdf1<sup>loxpl/loxpl</sup>CDX2-cre*) and initiated CRC in these mice by AOM/DSS treatment (figure 3A). We found that the overexpression of *Ythdf1* resulted in increased colon tumour number and size in the AOM/DSS model (figure 3C). Flow cytometry revealed increased MDSC infiltration together with reduced NK, *CD4<sup>+</sup>* T and *CD8<sup>+</sup>* T cells in colon tumours of *Ythdf1* knockin mice compared with wildtype mice (figure 3D). Moreover, we found that *Ythdf1* knockin reduced the proportion of functional T cells as identified by granzyme B, INF- $\gamma$  and TNF- $\alpha$  expression (figure 3E).

We next sought to validate these results in *Apc<sup>Min/+</sup>*-driven spontaneous CRC (figure 3B) by establishing *Apc<sup>Min/+</sup>Ythdf1<sup>loxpl</sup>* mice. Consistently, *Apc<sup>Min/+</sup>* mice with intestine-specific knockin of *Ythdf1* developed significantly bigger colon tumours than their wild-type littermates (figure 3C). Analysis

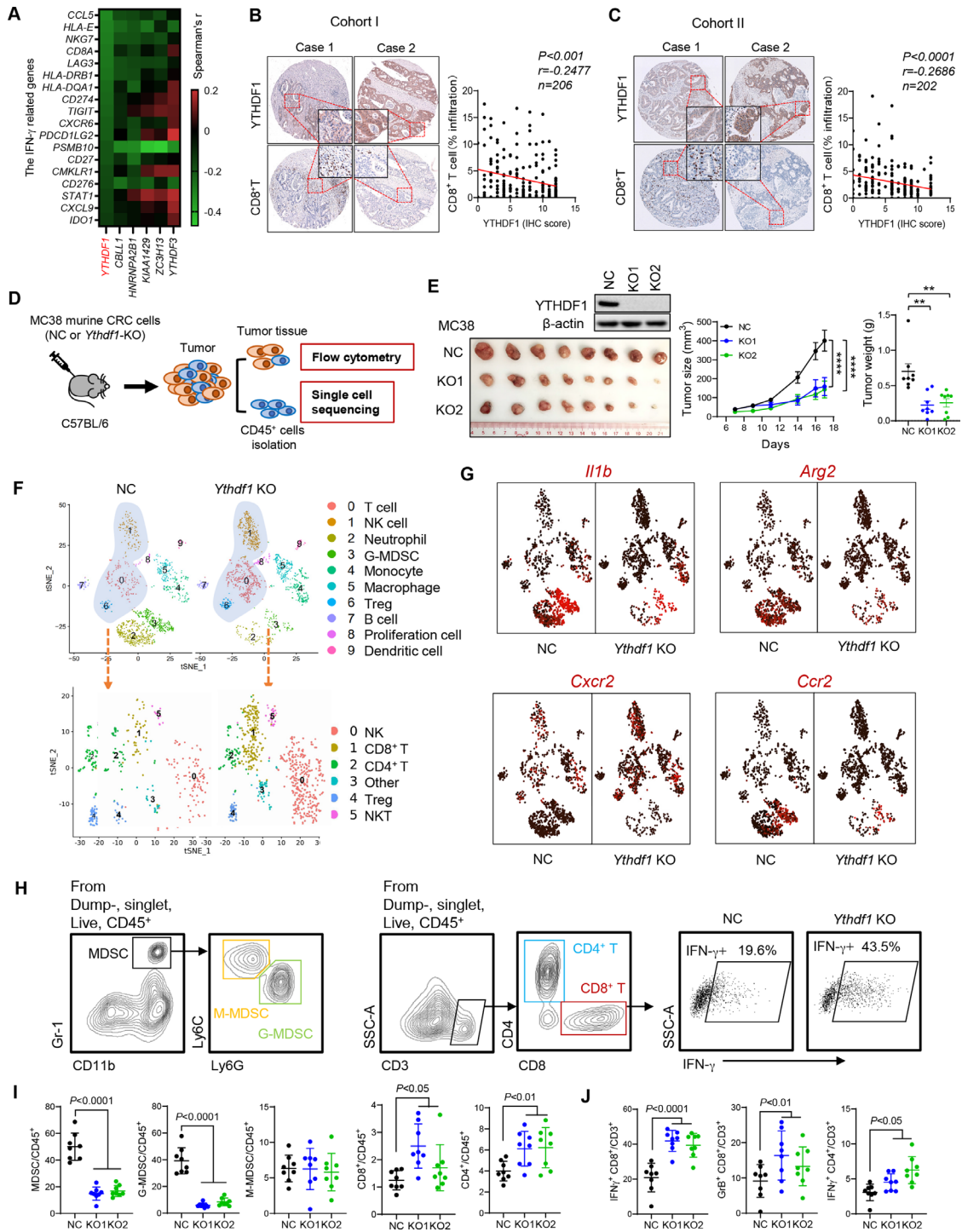


**Figure 1** YTH N<sup>6</sup>-methyladenosine RNA binding protein 1 (YTHDF1) is associated with an immunosuppressive microenvironment in patients with colorectal cancer (CRC) and its validation by scRNA-seq in immunocompetent mice. (A) Spearman's correlation in mRNA expression between interferon gamma (IFN- $\gamma$ )-related genes and m<sup>6</sup>A regulators in The Cancer Genome Atlas dataset. (B) Correlation between protein levels of YTHDF1 and CD8<sup>+</sup> T cell infiltration was determined by immunohistochemistry staining in cohort I ( $p < 0.0001$ ,  $r = -0.2686$ ,  $n = 202$ ), and (C) validation in cohort II ( $p < 0.001$ ,  $r = -0.2477$ ,  $n = 206$ ). (D) Experimental design for single-cell analysis of CD45<sup>+</sup> cells sorted from the tumours with or without *Ythdf1* by FACS, followed by droplet-enabled scRNA-seq. NC: cells with control sgRNA. *Ythdf1*-KO: cells with CRISPR knockout of *Ythdf1*. (E) Representative image (left), tumour volume (middle), and weight (right) of MC38 syngeneic tumours with or without *Ythdf1* knockout injected in C57BL/6 mice. (F) Upper panel: tSNE plot showing the components of immune cells in MC38 syngeneic tumours with or without *Ythdf1* knockout. Each dot represents a single cell. The same cell type was colour coded. Lower panel: subset analysis of T cell and NK cell clusters shown in tSNE projection regions. (G) Feature plots of characteristic markers of all cell types showing expression levels with low expression in dark red to high expression in bright red. (H) Gating strategies for flow cytometry. Identification of myeloid-derived suppressor cells (MDSC), M-MDSC, and G-MDSC (left). Identification of CD8<sup>+</sup> T and CD4<sup>+</sup> T cells (middle). Representative images showing increase of IFN- $\gamma$ <sup>+</sup> CD8<sup>+</sup> T cells in *Ythdf1*-KO tumours in (D) (Right). (I) Flow cytometry analysis performed with tumours derived from the indicated cells in (D) (\*\* $p < 0.01$ ; \*\*\*\* $p < 0.0001$ ) (linear regression (B, C), two tailed t-test (E, H, I), analysis of variance test (E)). NC: cells with control sgRNA. KO1: cells with *Ythdf1* sgRNA #1. KO2: cells with *Ythdf1* sgRNA #2. GrB: granzyme B.

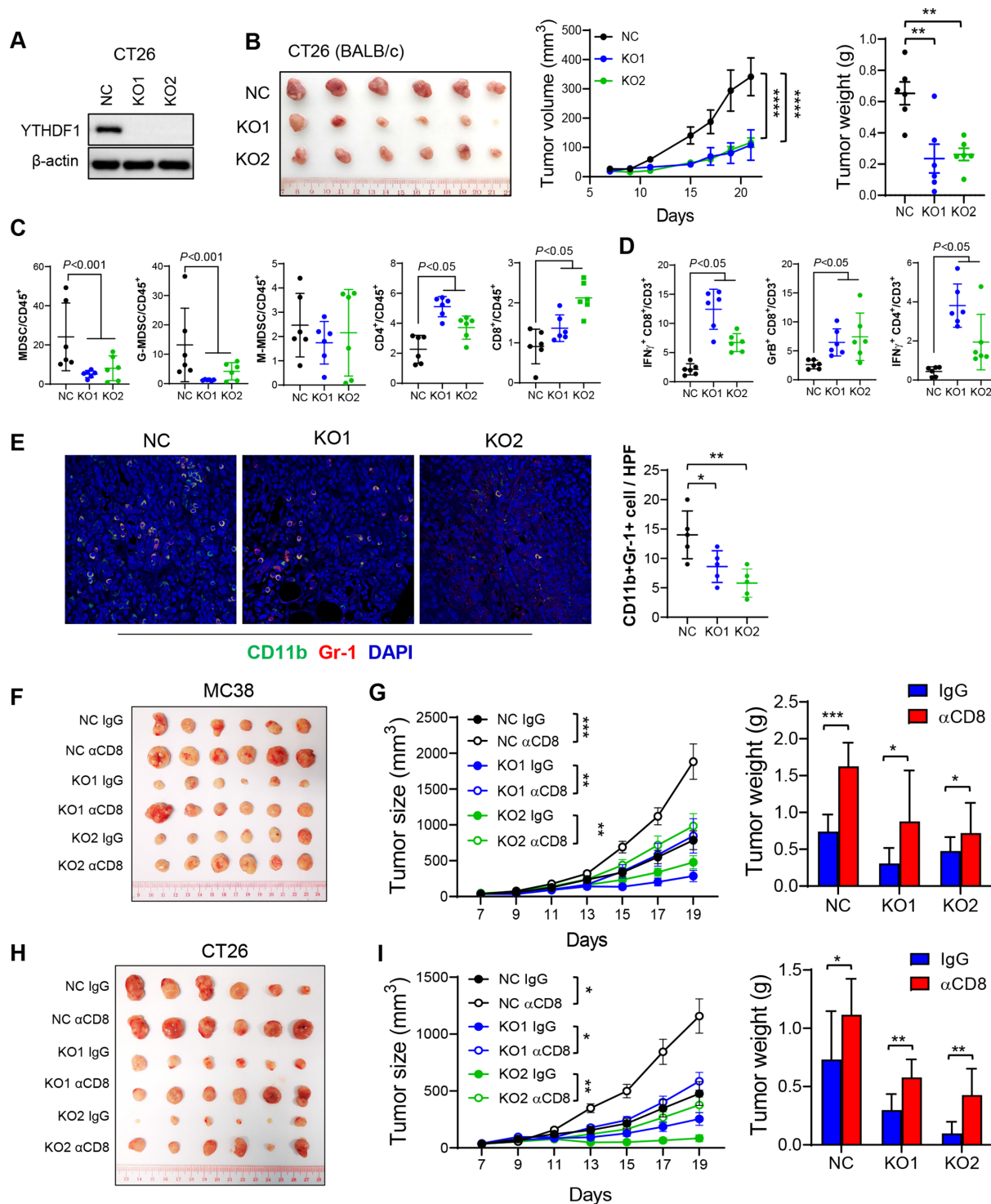


**Figure 2** YTH N<sup>6</sup>-methyladenosine RNA binding protein 1 (*Ythdf1*) knockout induces antitumour immunity by reduction of myeloid-derived suppressor cell (MDSC) and increase of functional T cells in syngeneic tumours, an effect reversed by CD8<sup>+</sup> T cell depletion. (A) Western blot validated *Ythdf1* knockout in CT26 cells. (B) Representative image of CT26 syngeneic tumours with or without *Ythdf1* Knockout (left). Knockout of *Ythdf1* in CT26 cells inhibits tumour growth (middle) and tumour weight (right) in BALB/c mice. (C) MDSC, G-MDSC, M-MDSC, CD4<sup>+</sup> T cells and CD8<sup>+</sup> T cells from tumours in (B) were analysed by flow cytometry. (D) Flow cytometry analysis assessing the percentage of T cell functional markers interferon gamma (IFN- $\gamma$ ) and granzyme B (GrB) from tumours in (B). (E) Immunofluorescence identifying MDSCs in subcutaneous tumours from BALB/c injected with the indicated CT26 cells (n=5 each group). (F) MC38 NC or *Ythdf1* knockout cells were implanted in C57BL/6 (n=6). Isotype control (IgG) or anti-mouse CD8 antibody ( $\alpha$ CD8) were given at 200  $\mu$ g/mouse on days 4, 7 and 9 post cell injection. Representative images of tumours from each group were shown. (G) Tumour volume (left) and weight (right) from tumours in (F). (H) CT26 NC or *Ythdf1* knockout cells were implanted in BALB/c (n=6). Isotype control (IgG) or  $\alpha$ CD8 were given at 200  $\mu$ g/mouse on days 4, 7 and 9 post cell injection. Representative images of tumours from each group were shown. (I) Tumour volume (left) and weight (right) from tumours in (H) (\*p<0.05; \*\*p<0.01; \*\*\*p<0.001; \*\*\*\*p<0.0001) (two tailed t-test (B, C, D, E, G, H), two-way analysis of variance test (D, G, I)). NC: cells with control sgRNA. KO1: cells with *YTHDF1* sgRNA #1. KO2: cells with *YTHDF1* sgRNA #2.

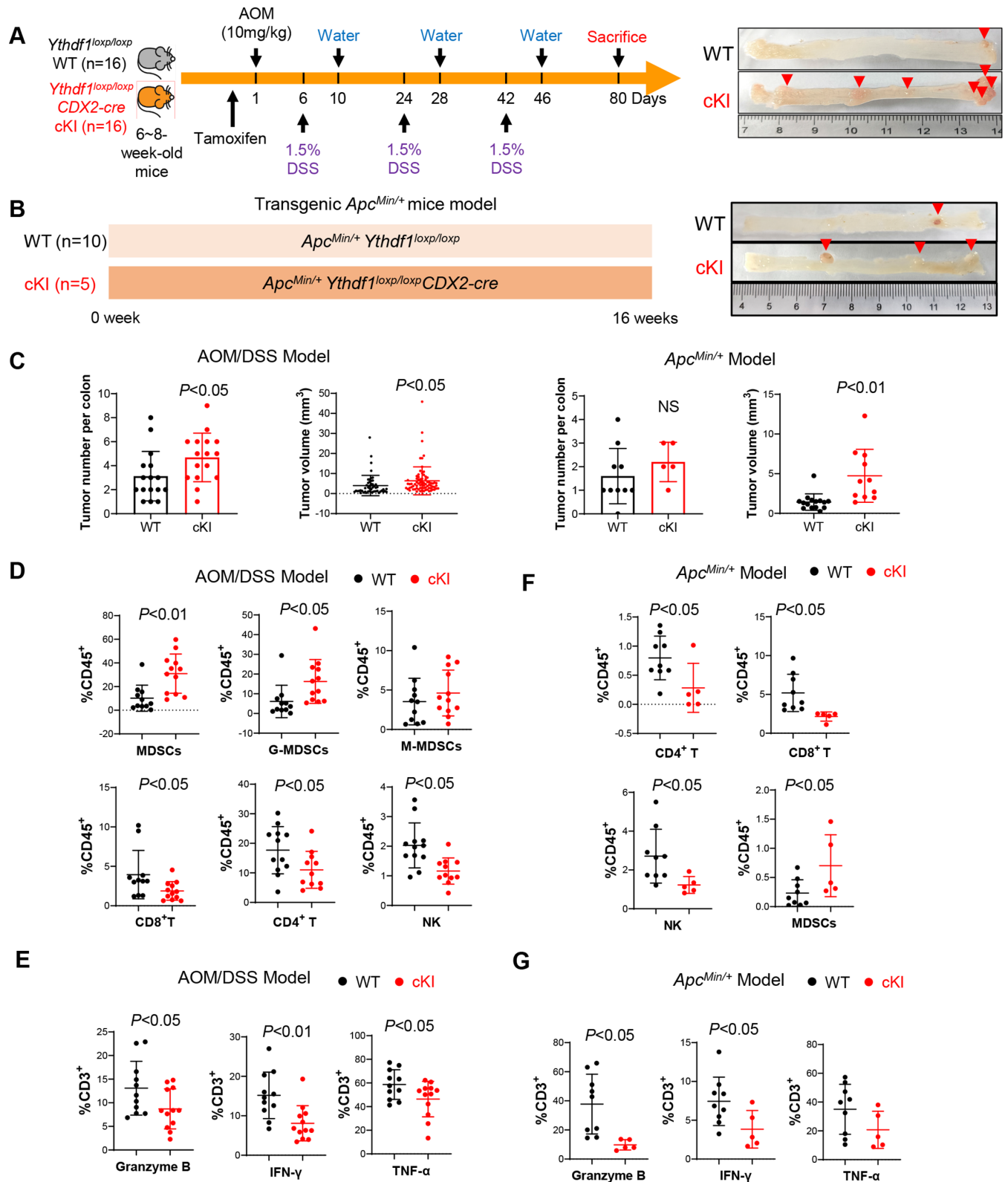


**Figure 3** Intestine-specific YTH<sup>N6</sup>-methyladenosine RNA binding protein 1 (*Ythdf1*) knockin promotes colorectal tumourigenesis and inhibits antitumour immunity in mice. (A) Scheme for azoxymethane-dextran sulphate-sodium (AOM/DSS) mouse model (left). Representative images of the colon at sacrifice (right). (B) Scheme for *Apc*<sup>Min/+</sup> mouse model (left). Representative images of the colon at sacrifice (right). (C) Tumour number, and tumour size in WT littermates (n=16) and *Ythdf1* Ki mice (n=16) mice treated with AOM-DSS (left). Tumour number, and tumour size in *Apc*<sup>Min/+</sup> *Ythdf1*<sup>loxp/loxp</sup> (n=10) and *Apc*<sup>Min/+</sup> *Ythdf1*<sup>loxp/loxp</sup> *CDX2-cre* mice (n=5) mice (right). (D) Infiltration of the indicated immune cells in tumours derived from AOM/DSS mice assessed by flow cytometry. (E) Composition of functional T cells in the tumours derived from AOM/DSS mice assessed by flow cytometry. (F) Infiltration of the indicated immune cells in the tumours derived from *Apc*<sup>Min/+</sup> mice assessed by flow cytometry. (G) Composition of functional T cells in the tumours derived from *Apc*<sup>Min/+</sup> mice assessed by flow cytometry. Two tailed t-test (C, E, F, G, H). WT: *Ythdf1* wild type; cKI: conditional *Ythdf1* knockin.

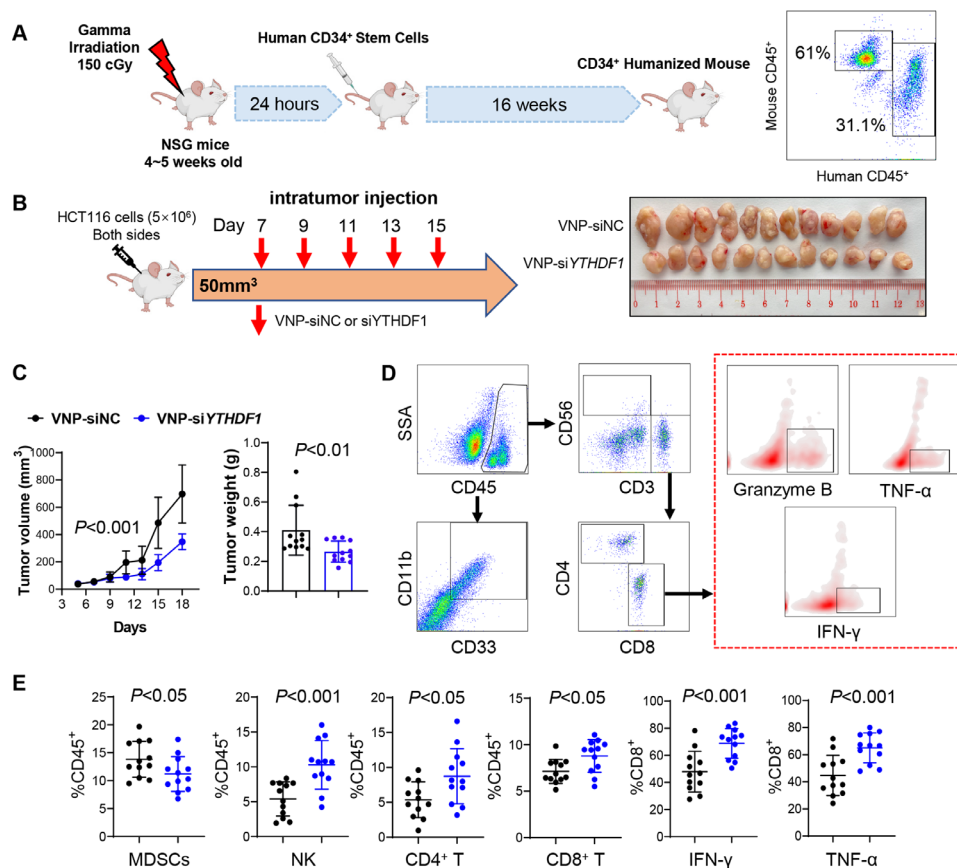


**Figure 4** VNP-siYTHDF1 boosted antitumour immunity in CD34<sup>+</sup> humanised mice. (A) Workflow for establishment of CD34<sup>+</sup> humanised mice (left). Percentage of human CD45<sup>+</sup> cells in the CD34<sup>+</sup> humanised mice was identified by flow cytometry (right). (B) Design for establishment of HCT116 xenografts and treatment with VNP-siNC or VNP-siYTHDF1 in CD34<sup>+</sup> humanised mice (left). Representative image of xenografts in different groups (right). (C) Tumour volume (left) and tumour weight (right) in mice in (B). (D) Gating strategies of immune cells in CD34<sup>+</sup> humanised mice. (E) Infiltration of CD4<sup>+</sup> T, CD8<sup>+</sup> T, NK cells, MDSCs and functional CD8 T cells was assessed by flow cytometry in the tumours from (B) (two tailed t-test (C, E), analysis of variance test (C)). VNP, vesicle-like nanoparticles.

of the tumour-infiltrating immune cells demonstrated remarkably decreased infiltration of NK, CD4<sup>+</sup> T and CD8<sup>+</sup> T cells in tumours with *Apc*<sup>Min/+</sup> with knockin of *Ythdf1*, together with the induction of MDSCs (figure 3F). Furthermore, *Ythdf1* knockin reduced granzyme B<sup>+</sup>, INF-γ<sup>+</sup>, or TNF-α<sup>+</sup> T cells in *Apc*<sup>Min/+</sup> mice (figure 3G). Collectively, these results support that YTHDF1 fosters an immunosuppressive microenvironment promoting spontaneous CRC.

#### Targeting YTHDF1 via VNP-siYTHDF1 boosts antitumour immunity in CD34<sup>+</sup> humanised mice

To confirm the role of YTHDF1 in modulating human antitumour immune response, we established the CD34<sup>+</sup> humanised mouse model.<sup>18</sup> Mice with peripheral blood mononuclear cells (PBMCs) comprising >20% human CD45<sup>+</sup> cells were used (figure 4A). To target YTHDF1 in vivo, we developed VNPs<sup>19</sup> to carry siRNA against YTHDF1. The humanised NSG mice bearing human CRC HCT116 xenografts were treated with VNP-siNC or -siYTHDF1 after tumours reached 50–100 mm<sup>3</sup> (figure 4B). VNP-siYTHDF1 significantly inhibited tumour volume and weight compared with VNP-siNC (figure 4B,C). We also performed flow cytometry to analyse the TIME (figure 4D). VNP-siYTHDF1 decreased MDSC infiltration, but increased CD4<sup>+</sup> T cell, CD8<sup>+</sup> T cell and NK cell accumulation (figure 4E). In addition, more IFN-γ<sup>+</sup>, TNF-α<sup>+</sup> and granzyme B<sup>+</sup> CD8<sup>+</sup> T cells were identified in tumours receiving VNP-siYTHDF1

(figure 4E). We also determined the safety of VNP-siYTHDF1 by measuring serum markers of liver (alanine aminotransferase and aspartate transaminase) and kidney function (creatinine and blood urea nitrogen). Mice treated with VNP-siNC or VNP-siYTHDF1 did not demonstrate abnormal liver or kidney function indicators (online supplemental figure S4), showing that VNP treatment is well tolerated. Thus, the targeting of YTHDF1 using VNP-siYTHDF1 is a safe and effective means to enhance antitumour immunity in humanised mice.

#### YTHDF1 promotes p65 translation to activate TNF/NF-κB signalling

To identify the molecular mechanism by which YTHDF1 elicits immunosuppression, we performed RNA-seq and Ribo-seq in CRC cells with or without knockout of YTHDF1. By RNA-seq analysis, differentially expressed genes between MC38-NC and MC38-YTHDF1-KO cells were enriched in TNF and NF-κB signalling pathways (online supplemental figure S5A). Consistent result was obtained in another CRC cell line CT26 showing that YTHDF1 regulated TNF/NF-κB signalling pathway (online supplemental figure S5B). In support of these, qPCR validated that *Ythdf1*-KO reduced mRNA expression of TNF/NF-κB targets (online supplemental figure S6A). Furthermore, Ribo-seq data revealed that loss of YTHDF1 was significantly associated with inactivation of TNF signalling (figure 5A). Accordingly, YTHDF1 knockout reduced ribosome protected fragment

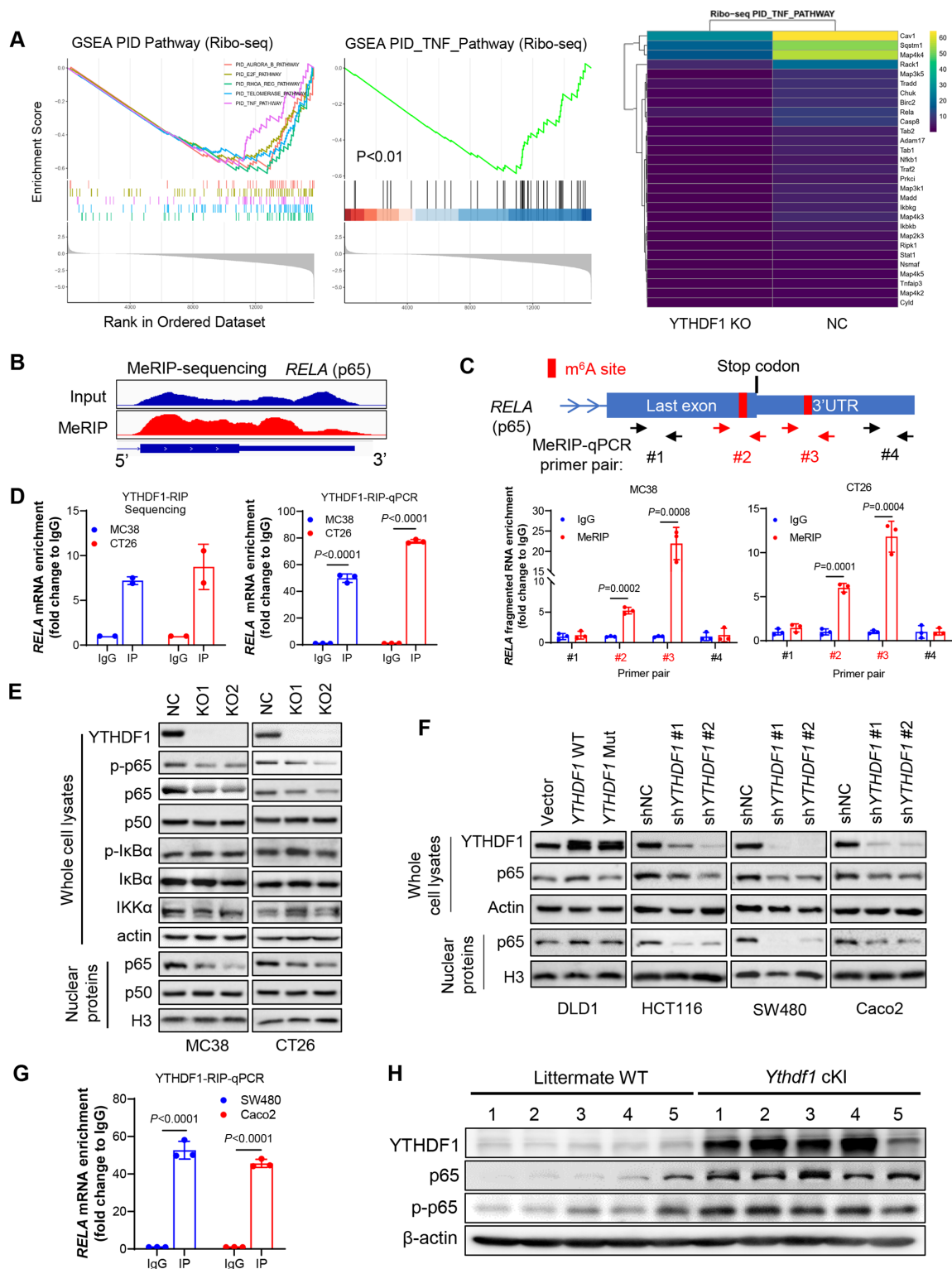


**Figure 5** YTH<sup>N6</sup>-methyladenosine RNA binding protein 1 (YTHDF1) promotes TNF/NF- $\kappa$ B signaling in CRC through promoting *RELA* (p65) mRNA translation. (A) Differentially expressed genes between CT26 cells with and without knockout of *Ythdf1* were enriched in TNF signalling pathway identifying by Ribo-seq (left). Heatmap of genes on TNF signalling pathway (right). (B) Methylated RNA immunoprecipitation (MeRIP) sequencing on CT26 cells, showing m<sup>6</sup>A modifications on last exon or 3'UTR of *RELA* (p65) mRNA. (C) Scheme showing the design of primers for MeRIP-qPCR to validate m<sup>6</sup>A modifications on p65 mRNA. Potential m<sup>6</sup>A sites were highlighted in red (upper). MeRIP-qPCR primers are indicated by arrows. MeRIP-qPCR validated m<sup>6</sup>A modification with primers #2 and #3 (lower). (D) RNA immunoprecipitation sequencing with anti-YTHDF1 antibody (YTHDF1-RIP) showing the enrichment of p65 mRNA compared with IgG control (left). YTHDF1-RIP-qPCR with primers specific to murine p65 mRNA (right). (E) Western blot of key effectors of TNF/NF- $\kappa$ B signalling pathway on knockout of *Ythdf1*. (F) Western blot analysis performed with indicated human CRC cells overexpressing wild-type (WT) or mutant (mut) *YTHDF1*, or *YTHDF1* knockdown with shRNA. Non-targeted shRNA (shNC) were used as control. (G) YTHDF1-RIP-qPCR with primers specific to human p65 mRNA. (H) Expression of p65 and phospho-p65 was determined by western blot in colon tumours from the intestine-specific *Ythdf1* knockin mice and wildtype littermates. cKI: conditional knockin (two tailed t-test (C, D, G)).



abundance of genes involved in TNF signalling (figure 5A). Thus, YTHDF1 could regulate TNF/NF- $\kappa$ B signalling by promoting protein translation. Since YTHDF1 functions as a m<sup>6</sup>A reader, we next performed m<sup>6</sup>A immunoprecipitation sequencing (MeRIP-seq) to pinpoint m<sup>6</sup>A-modified transcripts. By screening m<sup>6</sup>A peaks in mRNAs involved in TNF signalling, we identified two m<sup>6</sup>A sites close to the stop codon of p65 mRNA (figure 5B), which was validated by MeRIP-qPCR (figure 5C). Importantly, we identified a direct interaction between YTHDF1 and p65 mRNA by RNA immunoprecipitation (RIP) sequencing and RIP-qPCR with anti-YTHDF1 antibody (figure 5D). Thus, p65 mRNA is a direct target of YTHDF1. We found that knockout of *Ythdf1* attenuated p65 protein expression, especially nuclear p65 expression, in both CT26 and MC38 cells, without affecting the expression of other regulators of NF- $\kappa$ B pathways such as IKK $\alpha$  and I $\kappa$ B $\alpha$  (figure 5E). Notably, mRNA expression of p65 was unchanged in *Ythdf1*-KO cells (online supplemental figure S6B), supporting that YTHDF1 regulates p65 primarily at the level of protein translation, which is in line with the reported YTHDF1 function of facilitating translation of its targets. Consistent results were obtained in human CRC cells showing that overexpression of wild-type *YTHDF1*, but not dysfunctional mutant,<sup>5,6</sup> elevated p65 protein expression; conversely, *YTHDF1* knockdown attenuated p65 protein in human CRC cells (figure 5F). RIP-qPCR using anti-YTHDF1 antibody also confirmed a direct interaction between YTHDF1 and p65 mRNA in human CRC cells (figure 5G). We next sought to validate the association of YTHDF1 and p65 in vivo. In *Ythdf1* knockin mice, both p65 and phospho-p65 protein were increased in colon tumours (figure 5H). Collectively, YTHDF1 promotes p65 protein expression to activate TNF and NF- $\kappa$ B signalling in vitro and in vivo.

### YTHDF1 promotes MDSC migration via p65-CXCL1 axis

To understand the link between YTHDF1-induced p65 and its immunosuppression, we performed a cytokine multiplex immunoassay for the detection of 23 different mouse cytokines in conditioned medium of CRC cells, tumour lysates, and serum from mice bearing syngeneic tumours. Among these cytokines, CXCL1 was consistently reduced by *Ythdf1*-KO (figure 6A), and this reduction of CXCL1 was confirmed by ELISA assay (figure 6B). CXCL1 has been reported as a transcriptional target of NF- $\kappa$ B signalling,<sup>20,21</sup> and it promotes MDSC chemotaxis via interaction with its receptor CXCR2.<sup>22–24</sup> Given that *Ythdf1*-KO reduced MDSC infiltration in CRC TIME, we asked whether YTHDF1 modulates MDSC migration. As such, in vitro MDSC migration assay was conducted. We found that conditioned medium from wild-type CRC cells enhanced MDSC migration, which was impaired by the knockout of *Ythdf1* (figure 6C). Blocking CXCL1-CXCR2 interaction by CXCR2 inhibitor SB265610 eliminated the difference between control and *Ythdf1*-KO culture supernatant in mediating MDSC migration (figure 6C). Thus, YTHDF1 promotes MDSC migration through CXCL1/CXCR2 axis. We next asked whether YTHDF1 could regulate *Cxcl1* mRNA expression. As expected, *Ythdf1* knockout significantly inhibited *Cxcl1* mRNA levels in murine (figure 6D) and human CRC cell lines (online supplemental figure S7A). Conversely, the overexpression of wild-type *YTHDF1*, but not its dysfunctional mutant, elevated *CXCL1* transcription and protein levels in human CRC cells (online supplemental figure S7A). NF- $\kappa$ B activators, such as TNF- $\alpha$  and IL-1 $\beta$ , have been reported to induce *CXCL1* expression.<sup>25</sup> We thus treated MC38 cells with TNF- $\alpha$  and measured *CXCL1* mRNA and secretion.

TNF- $\alpha$  stimulated *Cxcl1* mRNA and secretion, an effect abrogated by the loss of *Ythdf1* (online supplemental figure S7B). To confirm the link between YTHDF1 and CXCL1 in human CRC, we examined the association between *YTHDF1* and *CXCL1* expression in TCGA CRC cohort. Consistently, *YTHDF1*-high CRC demonstrated high *CXCL1* expression (online supplemental figure S7C). Besides *CXCL1*, *CXCL2* also positively correlated with *YTHDF1* (online supplemental figure S7C). In contrast, *CXCL5* and *CXCL8* expression negatively correlated with *YTHDF1* (online supplemental figure S7C). Considering the role of YTHDF1 in promoting MSDC infiltration, we next performed CRC TMA of CD33, a marker for G-MDSCs.<sup>26,27</sup> We found that YTHDF1 protein levels positively correlated with the proportion of intratumoural CD33<sup>+</sup> cells (online supplemental figure S8). Our findings thus support a YTHDF1-p65-CXCL1/CXCR2 axis mediating MDSC migration in CRC.

We next investigated if YTHDF1 affects MDSC function. CD11b<sup>+</sup>Gr-1<sup>+</sup> MDSCs were isolated from MC38 syngeneic tumours and then cocultured with T cells in vitro (figure 6E). MDSCs isolated from control tumours suppressed T cell proliferation; however, MDSCs from *Ythdf1*-KO tumours exhibited significantly less suppressive activity against the proliferation of both CD8<sup>+</sup> T cells and CD4<sup>+</sup> T cells compared with MDSCs from the control (figure 6F,G). In support of this, MDSCs isolated from *Ythdf1*-KO tumours have reduced expression of MDSC functional markers *Nos2*, *Arg1*, and *Cd274* compared with *Ythdf1*-WT tumours (online supplemental figure S9A). Flow cytometry confirmed that iNOS<sup>+</sup> MDSCs was attenuated *Ythdf1*-KO tumours (online supplemental figure S9B). These data validate the reported immunosuppressive function of MDSCs on key effector cells, including CD8<sup>+</sup> T cells and CD4<sup>+</sup> T cells,<sup>28</sup> and support that *YTHDF1*-expressing CRC recruits functional MDSCs.

### YTHDF1 is a potential therapeutic target for CRC immunotherapy

Considering that reduced infiltration of MDSCs has been reported to correlate with enhanced immunotherapeutic efficacy in various cancer types,<sup>22,29,30</sup> we sought to test if targeting YTHDF1 augments anti-PD1 therapy in CRC. As expected, we found that knockout of *Ythdf1* boosted efficacy of anti-PD1 in MC38 (MSI-H) syngeneic tumours and prolonged survival of the tumour-bearing mice (figure 7A). We further exploited the VNPs system to deliver specific *Ythdf1*-siRNA into tumours. When MC38 syngeneic tumours reached 50~100 mm<sup>3</sup>, we treated the mice with VNP-si*Ythdf1* (or VNP-siNC) and anti-PD1 treatment (or IgG). VNP-si*Ythdf1* significantly suppressed MC38 tumour growth compared with VNP-siNC (figure 7B,C). Remarkably, the combination of VNP-si*Ythdf1* plus anti-PD1 exerted the strongest inhibitory effect against tumour growth (figure 7B,C).

We further addressed if targeting YTHDF1 can overcome anti-PD1 resistance in MSS CRC based on syngeneic CT26 (MSS CRC) tumour model. CT26 cells with *Ythdf1* knockout were thus injected to the syngeneic mice and treated with anti-PD1. We found that knockout of *Ythdf1* significantly enhanced anti-PD1 treatment efficacy in CT26 syngeneic tumours, which otherwise were non-responsive to ICB therapy (figure 7D,E).

Flow cytometry analysis further revealed that combination of *Ythdf1* silencing and anti-PD1 remarkably increased tumour-infiltrating functional CD8<sup>+</sup> T cells, including IFN- $\gamma$ <sup>+</sup> CD8<sup>+</sup> T cells and Granzyme B<sup>+</sup> CD8<sup>+</sup> T cells in both CT26 and MC38 syngeneic models (figure 7F,G). Furthermore, combinational treatment strongly reduced accumulation of MDSCs, whereas

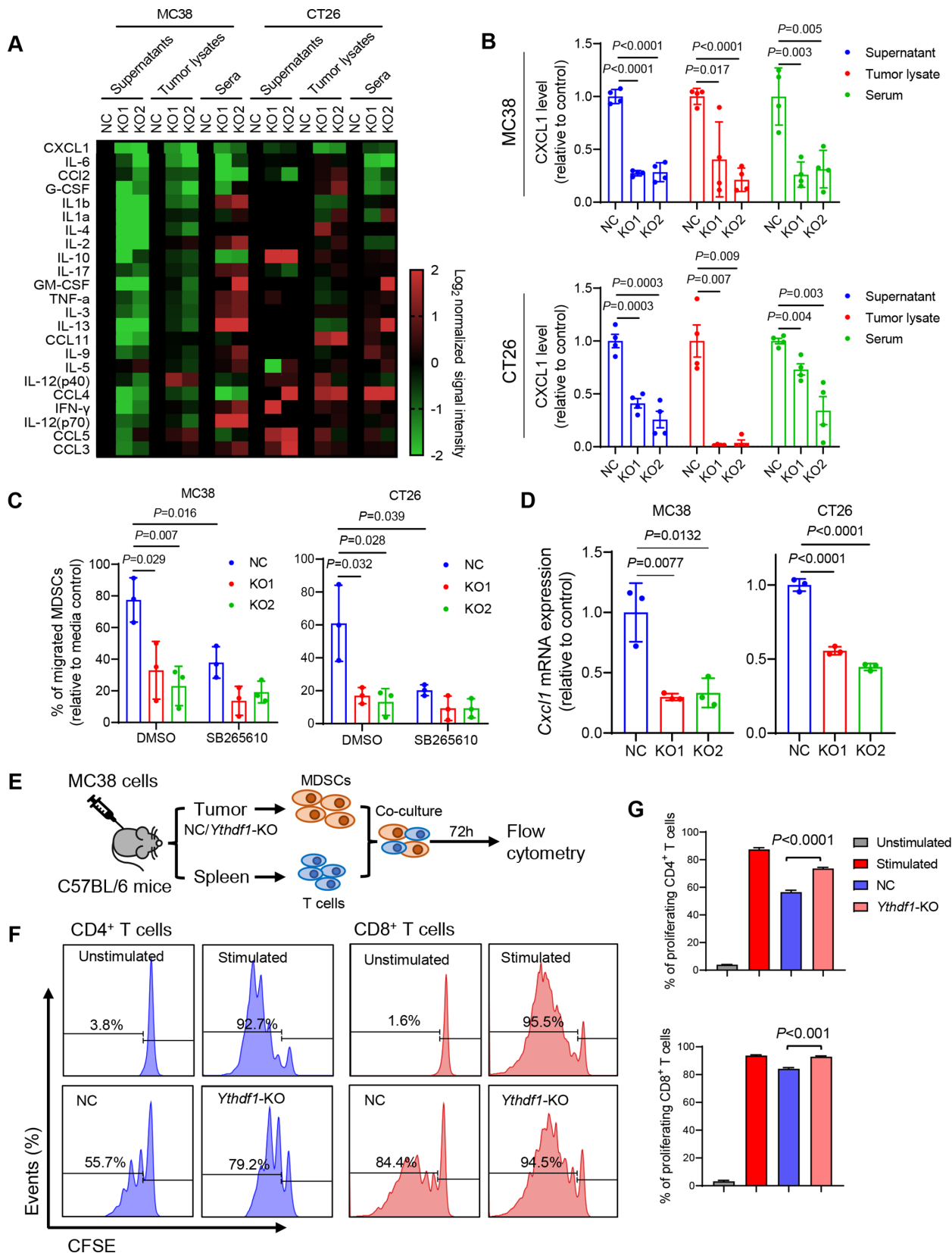


**Figure 6** Loss of YTH N<sup>6</sup>-methyladenosine RNA binding protein 1 (*Ythdf1*) promotes reduction of myeloid-derived suppressor cells (MDSCs) by decreasing CXCL1 secretion. (A) Multiplex mouse cytokine immunoassay assessing levels of 23 cytokines in cell culture supernatants from MC38 and CT26 cell culture, and tumour lysates and sera from MC38 and CT26 syngeneic tumour models. (B) ELISA validation of levels of CXCL1 in the indicated materials as in (A) (n=4 each group). (C) MDSC migration was assessed in vitro with transwell migration assay using conditional medium derived from the indicated cells. CXCR2 inhibitor SB265610 was used at 5  $\mu$ M. (D) RT-qPCR determination of *Cxcl1* mRNA expression in the indicated cells. (E) Flow chart of T cell suppression assay. (F) Representative images of flow cytometry assessing the proliferation of CFSE-labelled T cells cocultured with MDSCs isolated as (E). (G) Quantification of (F) (two tailed t-test (C, D, E, G)).

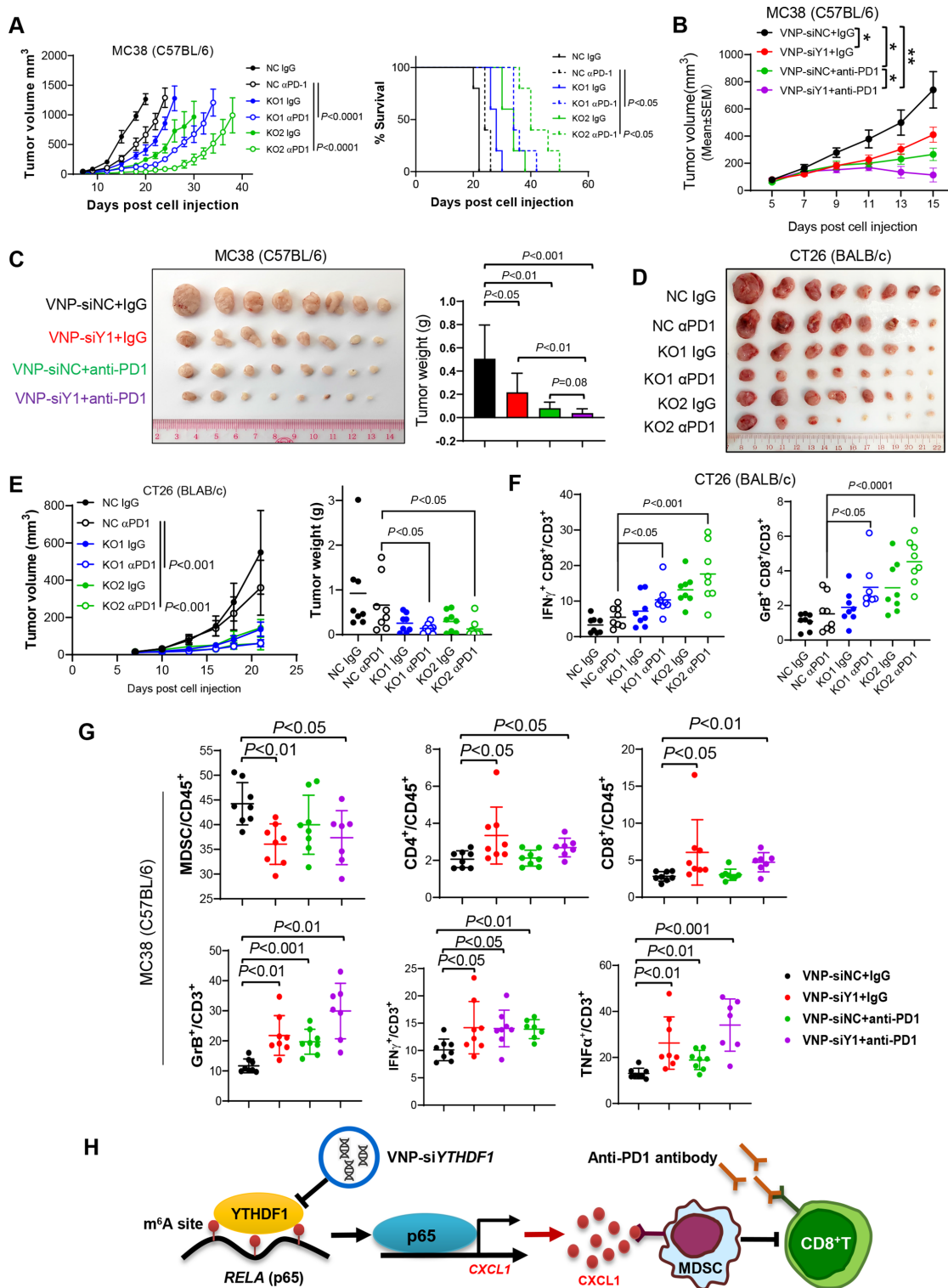


**Figure 7** Targeting YTH<sup>N6</sup>-methyladenosine RNA binding protein 1 (*YTHDF1*) augmented anti-PD1 blockade therapy in both microsatellite instability-high (MSI-H) and microsatellite stable colorectal cancer (CRC). (A) MC38 cells with or without *Ythdf1* knockout were implanted into C57BL/6 mice and treated with IgG or anti-PD1 ( $\alpha$ PD1; n=5 per group). Tumour volume (left) and mice survival (right) were presented. Euthanasia was applied when tumour burden was greater than or equal to 1500 mm<sup>3</sup> or when the mouse was moribund. (B) Growth curve of subcutaneous tumours from C57BL/6 injected with MC38 and treated with the indicated treatments. Vesicle-like nanoparticle (VNP)-siRNAs were given intratumorally. And  $\alpha$ PD1 was given with intraperitoneal injection. (C) Images and weight of the tumours from (B). (D) The indicated CT26 cells were subcutaneously injected in BALB/c mice. The mice were treated with control or  $\alpha$ PD1 (n=8 each group). Tumours removed from the mice at sacrifice were shown. (E) Tumour growth curve (left) and tumour weight (right) in (D). (F) Flow cytometry performed with the tumours in (D). (G) Top panel: flow cytometry assessing the proportion of MDSCs, CD4<sup>+</sup> T cells, and CD8<sup>+</sup> T cells in total CD45<sup>+</sup> cells in tumours in (B). Lower panel: flow cytometry assessing functional CD8<sup>+</sup> T cells in tumours in (B). (H) Schematic of the m<sup>6</sup>A-YTHDF1-p65-CXCL1 axis inducing MDSC accumulation and hence suppressing T cell function in CRC (two tailed t-test (C, D, F, G, H); analysis of variance test (A, C, F); long-rank test (A)). siY1: si*YTHDF1*. GrB: granzyme B.

CD4<sup>+</sup> T cells and CD8<sup>+</sup> T cells were induced (figure 7G). Thus, targeting of YTHDF1 not only potentiates ICB therapeutic efficacy in MSI-H CRC, but also overcomes ICB resistance in MSS CRC by suppressing recruitment of MDSCs and improving functionality of CD8<sup>+</sup> T cells.

## DISCUSSION

YTHDF1 is a m<sup>6</sup>A reader is frequently upregulated in CRC, but its role in antitumour immunity is largely unknown. Here, our study demonstrates for the first time that high YTHDF1 expression in CRC drives immunosuppression. Single-cell profiling reveals that YTHDF1 is crucial to the recruitment of MDSCs, which in turn attenuated T cell infiltration and function in CRC. This phenomenon is consistently found in syngeneic tumours, intestine-specific *Ythdf1* knockin mice and CD34<sup>+</sup> humanised mice. Taken together, our data demonstrate that YTHDF1 promotes an immunosuppressive tumour microenvironment to facilitate CRC tumourigenesis.

A series of in vivo models validated the role of YTHDF1 in recruitment of MDSCs in CRC. In CRC syngeneic models, *Ythdf1* knockout inhibited MDSC accumulation. Conversely, intestine-specific *Ythdf1* knockin accelerated colorectal tumourigenesis in AOM/DSS and *Apc*<sup>Min/+</sup> models, concomitant with increased intratumoural MDSCs. Moreover, *YTHDF1* silencing also impaired infiltration of human MDSCs in CD34<sup>+</sup> humanised mice. MDSCs are a highly diverse population of immature myeloid cells, including granulocytic MDSCs and monocytic MDSCs. Both of them, especially G-MDSCs, possess potent immunosuppressive activity.<sup>31</sup> In vitro MDSC migration assays directly validated that YTHDF1 plays a crucial role in MDSC chemotaxis. Our results support that YTHDF1 promotes colorectal tumourigenesis via MDSC-mediated immunosuppression.

MDSCs primarily exert their immunosuppressive effect by inhibiting key effector cell proliferation and activation.<sup>28</sup> Indeed, we found that *Ythdf1* knockout induces infiltration of CD4<sup>+</sup> T-cells, CD8<sup>+</sup> T cells and NK cells in CRC tumours and CD34<sup>+</sup> humanised mice, with increased expression of cytotoxic markers granzyme B, INF- $\gamma$  and TNF- $\alpha$  whereas intestine-specific *Ythdf1* knockin correlated with dampened infiltration and activity status of these effector cells. In vitro studies also demonstrated that MDSCs isolated from *Ythdf1*-null tumours have impaired capacity to suppress T cell proliferation. Together, our data support that YTHDF1-driven functional MDSC accumulation exerts an inhibitory effect on antitumour immune cells to promote immune evasion in CRC.

We next deciphered the molecular basis of YTHDF1-driven MDSC accumulation in CRC. As YTHDF1 functions as a m<sup>6</sup>A reader, we performed integrative RNA-seq, Ribo-seq and MeRIP-seq to identify candidate targets of YTHDF1 in CRC. Although several signalling pathways were identified in MSS (CT26) and MSI-H (MC38) CRC, TNF/NF- $\kappa$ B signalling pathway is the top pathway commonly induced by YTHDF1 in both models. We further unravelled p65 subunit of NF- $\kappa$ B as a direct target of YTHDF1. YTHDF1, but not its dysfunctional mutant, binds to m<sup>6</sup>A-modified p65 mRNA to increase p65 protein levels without affecting its mRNA expression, implying that YTHDF1 promotes p65 translation in m<sup>6</sup>A-dependent manner. TNF/NF- $\kappa$ B signalling is often activated in tumour cells, and induces expression of proinflammatory genes encoding cytokines and chemokines.<sup>32</sup> By cytokine profiling, we found that CXCL1 mRNA expression and secretion were unanimously repressed by genetic inhibition of *Ythdf1* in mouse

and human CRC cell lines, syngeneic mice and transgenic mice. CXCL1 plays a pivotal role in promoting MDSCs chemotaxis in TIME via interaction with CXCR2.<sup>33</sup> In line with this, we found that YTHDF1 mediates the migration of MDSCs via a CXCL1-CXCR2 axis, an effect abolished by a CXCR2 inhibitor. Together, YTHDF1-mediated p65 signalling promotes MDSCs via CXCL1 secretion. Apart from CXCL1, alternative NF- $\kappa$ B downstream targets were also down-regulated by *Ythdf1* knockout. It will be of interest to further explore the collateral impact of YTHDF1 on NF- $\kappa$ B-dependent expression of cytokines and chemokines on the immunosuppressive TIME of CRC.

MDSCs have been reported to exert immunosuppressive function on key effector cells, including CD8<sup>+</sup> T cells, CD4<sup>+</sup> T cells and NK cells.<sup>28</sup> MDSCs exert their antagonistic effect on antitumour T cells via a myriad of mechanisms, including depletion of intratumoural arginine via Arginase-1, induction of oxidative stress via iNOS, and secretion of immunosuppressive molecules such as TGF- $\beta$ .<sup>31</sup> Here, we showed that depleting *Ythdf1* in cancer cells suppressed intratumoural MDSCs and mitigated the immunosuppressive function of MDSCs on effector cells. MDSCs and T cell coculture studies demonstrated that MDSCs from *Ythdf1*-KO tumours have impaired capacity to suppress the cell proliferation of both CD8<sup>+</sup> T cells and CD4<sup>+</sup> T cells when compared with control tumours. Our findings thus support that YTHDF1 mediates the recruitment of functional MDSCs, which inhibit the function and proliferation of effector T cells in CRC, leading to compromised immune surveillance (figure 7H).

In the clinic, ICI therapy only shows beneficial effects to a small proportion of patients with MMR or MSI-H metastatic CRC, whereas the majority of CRCs with MSS status are largely non-responsive.<sup>34</sup> This can be partially attributed to presence of MDSCs and the formation of immunosuppressive tumour microenvironment. Given that knockout of *Ythdf1* reduced MDSC infiltration in CRC tissues to revert immune suppression, we thus explored therapeutic implications of targeting YTHDF1 in both MC38 (MSI-H) and CT26 (MSS) syngeneic CRC models. *Ythdf1* silencing boosted the anti-PD1 efficacy in MC38 syngeneic model. More importantly, targeting of YTHDF1 reversed anti-PD1 resistance in CT26 (MSS) syngeneic model, highlighting the broad utility of YTHDF1-targeting approach in promoting ICB efficacy not only in MSI-H CRC, but also MSS CRC that otherwise is resistant to ICB therapy.

As there is no currently available drug for YTHDF1, here we developed a nanoparticle-based delivery system<sup>35</sup> to deliver *YTHDF1*-siRNA in vivo. In syngeneic mouse models and humanised mice models of CRC, we observed the robust effect of VNP-si*YTHDF1* that remarkably elevated the infiltration of functional T cells and enhanced tumour response to anti-PD1 therapy. Targeting of YTHDF1 thus represents a promising immunotherapeutic target in CRC.

In conclusion, YTHDF1 expression in CRC recruits immunosuppressive MDSCs via activating m<sup>6</sup>A-p65-CXCL1 axis to inhibit T cells, thereby promoting CRC. Targeting YTHDF1 plus anti-PD1 therapy demonstrates promising antitumour efficacy against CRC, corroborating that YTHDF1 is a potential therapeutic target for CRC.

**Contributors** YB and JZ performed the experiments, analysed the data and drafted the manuscript. HC and CCW commented on the study and revised the paper. CL performed animal experiments. YD and DH performed bioinformatics analyses. HG, DC and YP performed experiments. WK and KFT performed histological staining and evaluation. JY designed and supervised the study and revised the manuscript. JY acts as the guarantor of the study.

**Funding** This study was supported by RGC Collaborative Research Fund (C4039-19GF), National Natural Science Foundation of China (81972576), RGC-GRF

(14110819, 14111621), RGC Research Impact Fund Hong Kong (R4032-21F), Vice-Chancellor's Discretionary Fund CUHK.

**Competing interests** None declared.

**Patient and public involvement** Patients and/or the public were not involved in the design, or conduct, or reporting, or dissemination plans of this research.

**Patient consent for publication** Not applicable.

**Ethics approval** This study was approved by Clinical Research Ethics Committee of the Chinese University of Hong Kong and Beijing Cancer Hospital.

**Provenance and peer review** Not commissioned; externally peer reviewed.

**Data availability statement** Data are available upon reasonable request.

**Supplemental material** This content has been supplied by the author(s). It has not been vetted by BMJ Publishing Group Limited (BMJ) and may not have been peer-reviewed. Any opinions or recommendations discussed are solely those of the author(s) and are not endorsed by BMJ. BMJ disclaims all liability and responsibility arising from any reliance placed on the content. Where the content includes any translated material, BMJ does not warrant the accuracy and reliability of the translations (including but not limited to local regulations, clinical guidelines, terminology, drug names and drug dosages), and is not responsible for any error and/or omissions arising from translation and adaptation or otherwise.

**Open access** This is an open access article distributed in accordance with the Creative Commons Attribution Non Commercial (CC BY-NC 4.0) license, which permits others to distribute, remix, adapt, build upon this work non-commercially, and license their derivative works on different terms, provided the original work is properly cited, appropriate credit is given, any changes made indicated, and the use is non-commercial. See: <http://creativecommons.org/licenses/by-nc/4.0/>.

#### ORCID iDs

Huarong Chen <http://orcid.org/0000-0003-2192-1864>

Wei Kang <http://orcid.org/0000-0002-4651-677X>

Jun Yu <http://orcid.org/0000-0001-5008-2153>

#### REFERENCES

- 1 Biller LH, Schrag D. Diagnosis and treatment of metastatic colorectal cancer: a review. *JAMA* 2021;325:669–85.
- 2 André T, Shiu K-K, Kim TW, et al. Pembrolizumab in microsatellite-instability-high advanced colorectal cancer. *N Engl J Med* 2020;383:2207–18.
- 3 Delaunay S, Frye M. Rna modifications regulating cell fate in cancer. *Nat Cell Biol* 2019;21:552–9.
- 4 Lin X, Chai G, Wu Y, et al. RNA m<sup>5</sup>a methylation regulates the epithelial mesenchymal transition of cancer cells and translation of snail. *Nat Commun* 2019;10:2065.
- 5 Pi J, Wang W, Ji M, et al. YTHDF1 promotes gastric carcinogenesis by controlling translation of FZD7. *Cancer Res* 2021;81:2651–65.
- 6 Liu T, Wei Q, Jin J, et al. The M6a reader YTHDF1 promotes ovarian cancer progression via augmenting eIF3c translation. *Nucleic Acids Res* 2020;48:3816–31.
- 7 Cerami E, Gao J, Dogrusoz U, et al. The cBio cancer genomics portal: an open platform for exploring multidimensional cancer genomics data. *Cancer Discov* 2012;2:401–4.
- 8 Gao J, Aksoy BA, Dogrusoz U, et al. Integrative analysis of complex cancer genomics and clinical profiles using the cBioportal. *Sci Signal* 2013;6:pl1.
- 9 Subramanian A, Tamayo P, Mootha VK, et al. Gene set enrichment analysis: a knowledge-based approach for interpreting genome-wide expression profiles. *Proc Natl Acad Sci U S A* 2005;102:15545–50.
- 10 Tigano M, Vargas DC, Tremblay-Belzile S, et al. Nuclear sensing of breaks in mitochondrial DNA enhances immune surveillance. *Nature* 2021;591:477–81.
- 11 Sun L, Kees T, Almeida AS, et al. Activating a collaborative innate-adaptive immune response to control metastasis. *Cancer Cell* 2021;39:1361–74.
- 12 Gao J, Shi LZ, Zhao H, et al. Loss of IFN- $\gamma$  pathway genes in tumor cells as a mechanism of resistance to anti-CTLA-4 therapy. *Cell* 2016;167:397–404.
- 13 Sharma P, Hu-Lieskovan S, Wargo JA, et al. Primary, adaptive, and acquired resistance to cancer immunotherapy. *Cell* 2017;168:707–23.
- 14 Ayers M, Luceford J, Nebozhyn M, et al. IFN- $\gamma$ -related mrna profile predicts clinical response to PD-1 blockade. *J Clin Invest* 2017;127:2930–40.
- 15 Cristescu R, Mogg R, Ayers M, et al. Pan-tumor genomic biomarkers for PD-1 checkpoint blockade-based immunotherapy. *Science* 2018;362:eaar3593.
- 16 Wang W, Green M, Choi JE, et al. Cd8+ T cells regulate tumour ferroptosis during cancer immunotherapy. *Nature* 2019;569:270–4.
- 17 Pagès F, Mlecnik B, Marliot F, et al. International validation of the consensus immunoscore for the classification of colon cancer: a prognostic and accuracy study. *Lancet* 2018;391:2128–39.
- 18 Choi Y, Lee S, Kim K, et al. Studying cancer immunotherapy using patient-derived xenografts (pdxs) in humanized mice. *Exp Mol Med* 2018;50:99.
- 19 Rezvantalab S, Drude NI, Moraveji MK, et al. PLGA-based nanoparticles in cancer treatment. *Front Pharmacol* 2018;9:1260.
- 20 Scortegagna M, Cataisson C, Martin RJ, et al. Hif-1 $\alpha$  regulates epithelial inflammation by cell autonomous Nf $\kappa$ pB activation and paracrine stromal remodeling. *Blood* 2008;111:3343–54.
- 21 Kemp SB, Carpenter ES, Steele NG, et al. Apolipoprotein E promotes immune suppression in pancreatic cancer through NF- $\kappa$ B-mediated production of CXCL1. *Cancer Res* 2021;81:4305–18.
- 22 Highfill SL, Cui Y, Giles AJ, et al. Disruption of CXCR2-mediated MDSC tumor trafficking enhances anti-PD1 efficacy. *Sci Transl Med* 2014;6:237ra67.
- 23 Wang D, Sun H, Wei J, et al. Cxcl1 is critical for premetastatic niche formation and metastasis in colorectal cancer. *Cancer Res* 2017;77:3655–65.
- 24 Zhang Q, Ma C, Duan Y, et al. Gut microbiome directs hepatocytes to recruit mdscs and promote cholangiocarcinoma. *Cancer Discov* 2021;11:1248–67.
- 25 Olivera I, Sanz-Pamplona R, Bolaños E, et al. A therapeutically actionable protumoral axis of cytokines involving IL-8, TNF $\alpha$ , and IL-1 $\beta$ . *Cancer Discov* 2022;12:2140–57.
- 26 Bronte V, Brandau S, Chen S-H, et al. Recommendations for myeloid-derived suppressor cell nomenclature and characterization standards. *Nat Commun* 2016;7:12150.
- 27 Cassetta L, Baekkevold ES, Brandau S, et al. Deciphering myeloid-derived suppressor cells: isolation and markers in humans, mice and non-human primates. *Cancer Immunol Immunother* 2019;68:687–97.
- 28 Veglia F, Sanseviero E, Gabrilovich DI. Myeloid-Derived suppressor cells in the era of increasing myeloid cell diversity. *Nat Rev Immunol* 2021;21:485–98.
- 29 Steele CW, Karim SA, Leach JDG, et al. CXCR2 inhibition profoundly suppresses metastases and augments immunotherapy in pancreatic ductal adenocarcinoma. *Cancer Cell* 2016;29:832–45.
- 30 Greene S, Robbins Y, Mydlarz WK, et al. Inhibition of MDSC trafficking with SX-682, a CXCR1/2 inhibitor, enhances NK-cell immunotherapy in head and neck cancer models. *Clin Cancer Res* 2020;26:1420–31.
- 31 Gabrilovich DI, Nagaraj S. Myeloid-Derived suppressor cells as regulators of the immune system. *Nat Rev Immunol* 2009;9:162–74.
- 32 Hoesel B, Schmid JA. The complexity of NF- $\kappa$ B signaling in inflammation and cancer. *Mol Cancer* 2013;12:86.
- 33 Kumar V, Patel S, Tcyganov E, et al. The nature of myeloid-derived suppressor cells in the tumor microenvironment. *Trends Immunol* 2016;37:208–20.
- 34 Overman MJ, Lonardi S, Wong KYM, et al. Durable clinical benefit with nivolumab plus ipilimumab in DNA mismatch repair-deficient/microsatellite instability-high metastatic colorectal cancer. *J Clin Oncol* 2018;36:773–9.
- 35 Mitchell MJ, Billingsley MM, Haley RM, et al. Engineering precision nanoparticles for drug delivery. *Nat Rev Drug Discov* 2021;20:101–24.